Engineering Fracture Mechanics 148 (2015) 383–405

Contents lists available at ScienceDirect

Engineering Fracture Mechanics

journal homepage: www.elsevier.com/locate/engfracmech

Fracture assessments of clad pipe girth welds incorporating improved crack driving force solutions

Rodolfo F. Souza, Claudio Ruggieri *

Department of Naval Architecture and Ocean Engineering, University of São Paulo, São Paulo, Brazil

ARTICLE INFO

Article history:
Received 17 September 2014
Received in revised form 5 March 2015
Accepted 27 April 2015
Available online 13 May 2015

Keywords:
J-integral
Fully-plastic solution
Reference stress
Defect assessment
Mismatch weld
Girth weld
Steel catenary riser

ABSTRACT

This work addresses an evaluation procedure for the *J*-integral in pipeline girth welds with circumferential surface cracks subjected to bending load for a wide range of crack geometries and weld mismatch levels based on the GE-EPRI and the reference stress framework. The study also addresses evaluation of critical flaw sizes for a subsea flowline clad pipe having an undermatched girth weld made of UNS N06625 Alloy 625. The 3-D numerical analyses provide a large set of *J*-solutions in cracked pipes with mismatched girth welds with implications of the potential applicability of ECA procedures in welded cracked structural components.

1. Introduction

The increasing demand for energy and natural resources has spurred a flurry of exploration and production activities of oil and natural gas in more hostile environments, including very deep water offshore hydrocarbon reservoirs. One of the key challenges facing the oil and gas industry is the assurance of more reliable and fail-safe operations of the infrastructure for production and transportation. Currently, structural integrity of submarine risers and flowlines conducting corrosive and aggressive hydrocarbons represents a key factor in operational safety of subsea pipelines. Advances in existing technologies favor the use of C–Mn steel pipelines, including API X65 and X70 grade steels, either clad or mechanically lined with corrosion resistant alloys (CRA), such as ASTM UNS N06625 Alloy 625 [1,2], for the transport of corrosive fluids.

A case of interest includes deep water steel catenary risers (SCRs) installed by the pipe reeling process which allows pipe welding and inspection to be conducted at onshore facilities. Here, the welded pipe is coiled around a large diameter reel on a vessel and then unreeled, straightened and finally deployed to the sea floor [3–6]. A key step in the reeled pipeline installation technique lies in the use of automatic ultrasound testing (AUT) during fabrication of girth welds, rather than radiography testing (RT), as the main inspection method thereby allowing a relatively straightforward application of standard fitness-for-service (FFS) procedures to determine tolerable flaw sizes [7]. However, a different picture emerges in the case of clad or lined pipe girth weld as fracture assessments and specification of critical flaw sizes for these components become more complex due to the dissimilar nature of the girth weld materials. Moreover, while faster and more practical,

* Corresponding author. Tel.: +55 11 30915184; fax: +55 11 30915717.
E-mail address: claudio.ruggieri@usp.br (C. Ruggieri).

http://dx.doi.org/10.1016/j.engfracmech.2015.04.029
0013-7944/

Nomenclature

α	Ramberg–Osgood dimensionless constant
α_{wm}	Ramberg–Osgood dimensionless constant for the weld metal
$\bar{\epsilon}$	true (logarithmic) strain
$\bar{\sigma}$	true stress
ϵ_p	plastic strain
ϵ_r	reeling strain
ϵ_{ref}	reference strain
ϵ_{ys}	yield strain
ϵ_{ys}^{wm}	weld metal yield strain
ϵ_z^b	longitudinal bending strain
$\widehat{K}_r$	applied toughness ratio
$\widehat{L}_r$	applied load ratio
ν	Poisson's ratio
σ^{bm}	true base metal stress
σ^{wm}	true weld metal stress
σ_0	yield (reference) stress
σ_b	bending stress
σ_{eq}	equivalent (effective) stress
σ_{ref}	reference stress
σ_{uts}	tensile strength
σ_{ys}	yield stress
σ_{ys}^{bm}	base metal yield stress
σ_{ys}^{wm}	weld metal yield stress
θ	crack length angle
$\tilde{\sigma}$	equivalent stress
ξ_n	coefficients of the polynomial fitting
a	crack depth
a_{cr}	critical crack depth size
b	remaining crack ligament
c	circumferential crack half-length
D_e	pipe outer diameter
E	Young's modulus
G_5	influence coefficient for a circumferential semi-elliptical surface crack
h	weld half width
h_1	nondimensional elastic–plastic parameter
J	J-integral
J_e	elastic component of the J-integral
J_{mat}	material's elastic–plastic toughness
J_{p-t}^{wm}	J_p-value corresponding to the limit bending moment using weld metal tensile stress
J_{p-y}^{wm}	J_p-value corresponding to the limit bending moment using weld metal yield stress
J_p	plastic component of the J-integral
K_r	normalized crack-tip loading
l	characteristic length
L_r	normalized load ratio
L_r^{max}	cut-off load ratio
M_b	bending moment
M_0^{wm}	limit bending moment for the all weld metal condition
M_y	mismatch ratio
n	Ramberg–Osgood strain hardening exponent
n_{wm}	Ramberg–Osgood strain hardening exponent for the weld metal
P	generalized load
P_0	generalized limit load
P_0^{bm}	limit load of the all base metal structure
P_0^{Mism}	limit load of the mismatched structure
P_0^{wm}	limit load of the all weld metal structure
Q_s	flaw shape parameter
R	reel radius
R_b	bending radius
R_e	pipe outer radius

R_i	pipe inner radius
R_m	pipe mean radius
t	pipe thickness
W	cracked component width
AUT	automatic ultrasound testing
CRA	corrosion resistant alloy
CTOD	crack tip opening displacement
ECA	engineering critical assessment
FAD	failure assessment diagram
HAZ	heat affected zone
RT	radiography testing
SCR	steel catenary riser
SGC	small geometry change

the reeling process subjects the pipe to large bending load and high tensile forces imposed on the pipeline with a strong impact on stable crack propagation of undetected flaws at girth welds thereby potentially leading to premature pipe failure.

Fracture mechanics based approaches, also referred to as Engineering Critical Assessment (ECA) procedures, provide a means to construct a correlation of crack size with applied loading as measured by the linear elastic stress intensity factor, K, or the elastic–plastic parameter defined by the J-integral and its corresponding value of the Crack Tip Opening Displacement, CTOD [8,9]. Further developments in the ECA methodology introduce a concise framework to explicitly address the potential interaction between stress-controlled cleavage fracture and plastic collapse to predict structural failure by adopting the concept of a failure assessment diagram (FAD) to evaluate the severity of crack-like flaws. The methodology thus provides a highly effective, albeit conservative, acceptance criterion for cracked structural components which relates the operating conditions with a critical applied load or critical crack size. Several flaw assessment procedures based upon the FAD concept, such as the R6 methodology [10], BS7910 [11], SINTAP [12] and API 579 [13], among others, are now well established and widely employed to analyze the significance of defects in terms of assessment of structural integrity. Zerbst et al. [14] provide an overview of analytical flaw assessment methods. While most ECA methodologies share a similar fracture mechanics spirit to ensure structural integrity and adequate safety margins, there are important differences depending on the adopted pipeline code.

Current onshore and cross-country pipeline construction codes in North America, such as API 1104 [15] and CSA Z662 [16], provide fracture assessment procedures for pipeline girth welds based on the concept of CTOD design curves. In particular, Annex C of CSA Z662, which builds on previous work of Wang and co-workers [17–20], defines a relationship between fracture toughness (as characterized by an *apparent* CTOD) and remote longitudinal strain for varying mechanical and geometrical parameters, including the ratio of yield strength to tensile strength, flaw size and flaw location. Here, a critical flaw size is determined for a given set of material properties and imposed level of (remote) strain.

Fracture assessment methodologies for offshore pipelines have evolved along a different line of development. The introduction of the first DNV OS-F101 [21] in 2000 marks the beginning of a now extensively used approach for assessing structural defects in girth welds of subsea pipelines and flowlines, including reeled pipelines. The current version of DNV OS-F101 [22] issued in 2013 became presumably the most comprehensive offshore pipeline code to cover design, construction and operation of offshore pipelines. Specifically, Appendix A of DNV OS-F101 [22] provides requirements and guidance for conducting an ECA analysis of girth welds in offshore pipelines, which are also supplemented by additional guidance provided by DNV RP-F108 [23] when the girth welds are subjected to cyclic plastic strains during installation.

The DNV ECA procedure to develop flaw acceptance criteria for pipeline girth welds relies almost entirely on the BS 7910 [11] approach for structural integrity assessments using the material-specific Option 2B or 3B with a number of amendments and small modifications, as detailed in Appendix A of [22], to allow proper treatment of strain-based loading conditions such as in reeled pipelines under high plastic strains. These amendments include the use of single edge tension notched specimens (most often referred to as SE(T) or SENT specimens) to the measure the material's fracture toughness, adoption of an upper-bound stress–strain curve with the lowest strain hardening as the input for the material-specific Option 2B or 3B assessment curve and the Kastner reference stress solution, among others (see also [7,24]).

While applications of FAD-based procedures have proven sufficiently effective in assessing the significance of structural defects in homogeneous materials, they do not necessarily provide reliable and accurate defect acceptance limits for welded components with weld metal strength mismatch. Here, mismatch in the flow properties between the weld metal and the base plate material alters the plastic deformation pattern of crack-like flaws that often occur in the weld metal and heat affected zone (HAZ) region thereby affecting the coupling relationship between remote loading and crack-tip loading (as characterized by J or the crack tip opening displacement – CTOD). Moreover, the changes in the evolving character of near-tip plastic deformation also affects the plastic collapse load of the cracked welded component. In particular, these features have important implications on structural integrity assessments of undermatched welds as, for a given remote loading,

crack-tip driving forces are higher and plastic collapse loads are lower when compared with the corresponding quantities evaluated for homogeneous materials. With the increased use of higher strength pipeline steels, unintended weld strength undermatching emerges as a likely possibility which thus raises strong concerns in integrity assessments of field girth welds having circumferential flaws.

This work focuses on the development of an evaluation procedure to determine the elastic–plastic crack driving force (as characterized by the J-integral) in pipeline girth welds with circumferential surface cracks subjected to bending load for a wide range of crack geometries and weld mismatch levels based upon the GE-EPRI framework and the reference stress approach. The objectives of the present investigation are twofold. First, the study broadens the applicability of current evaluation procedures for J which enter directly into structural integrity analyses and flaw tolerance criteria to provide numerical solutions for crack driving forces in mismatched girth welds with circumferential surface cracks. As a second objective, we analyze the potential effects of an undermatched girth weld on critical flaw sizes for a typical clad pipe employed in subsea flowlines having a girth weld made of UNS N06625 Alloy 625. Attention is given here to structural integrity analyses derived from three related ECA procedures incorporating the GE-EPRI framework and the reference stress approach. The extensive nonlinear, 3-D numerical analysis provide a large set of solutions for J in cracked pipes and cylinders with mismatched girth welds while, at the same time, gaining additional understanding of the potential applicability of ECA procedures in welded cracked structural components.

2. The GE-EPRI evaluation methodology

A convenient methodology to estimate the J Integral for a cracked component such as a circumferentially cracked pipe (the procedure to estimate the CTOD is analogous but it is not addressed here in interest of space - readers are referred to the work of Chiodo and Ruggieri [25] for further details) derives from the fully plastic description of J based upon HRR-controlled crack-tip fields [8] and limit load solutions for a strain hardening material introduced by Shih and Hutchinson [26] and further validated by Kumar et al. [27] (see also Kanninen and Popelar [28]). The procedure begins by considering the elastic and plastic contributions to the J-integral as

$$J = J_e + J_p \tag{1}$$

where the elastic component, J_e, is given by the standard form

$$J_e = \frac{K_I^2}{E'} \tag{2}$$

in which K_I is the (Mode I) elastic stress intensity factor and $E' = E$ or $E' = E/(1-\nu^2)$ whether plane stress or plane strain conditions are assumed with E representing the (longitudinal) elastic modulus ans ν is the Poisson's ratio.

For an elastic–plastic material obeying a Ramberg–Osgood model [9,29] to describe the uniaxial true stress ($\bar{\sigma}$) vs. logarithmic strain ($\bar{\epsilon}$) response given by

$$\frac{\bar{\epsilon}}{\epsilon_{ys}} = \frac{\bar{\sigma}}{\sigma_{ys}} + \alpha\left(\frac{\bar{\sigma}}{\sigma_{ys}}\right)^n \tag{3}$$

where α is a dimensionless constant, n defines the strain hardening exponent, σ_{ys} and $\epsilon_{ys} = \sigma_{ys}/E$ define the yield stress and strain, the plastic component, J_p, is expressed as

$$J_p = \alpha\epsilon_{ys}\sigma_{ys}b[h_1(a/W,\ \ell,\ n)]\left(\frac{P}{P_0}\right)^{n+1} \tag{4}$$

where a is the crack size, W denotes the cracked component width, $b = W - a$ defines the uncracked ligament, ℓ represents a characteristic length for the cracked component, P is a generalized load and P_0 denotes the corresponding (generalized) limit load. In the above expression, h_1 is a dimensionless factor dependent upon crack size, component geometry and strain hardening properties. The previous solution for J_p became widely known as the GE-EPRI methodology [27,30]. Recent work of Chiodo and Ruggieri [25] has expanded these J solutions to include a wide range of circumferentially cracked pipes subjected to bending with varying crack geometries and strain hardening properties applicable to homogeneous materials.

To introduce an estimation procedure for J_p in a cylinder or pipe having a circumferential surface crack located at the girth weld centerline based upon the previous fully-plastic solution, consider the crack configuration subjected to bend loading illustrated in Fig. 1, in which $2h$ represents the weld groove width. Moreover, to facilitate development of the fully plastic solution for J_p incorporating effects of weld strength mismatch, it proves convenient to first define the mismatch ratio, M_y, as

$$M_y = \frac{\sigma_{ys}^{wm}}{\sigma_{ys}^{bm}} \tag{5}$$

where σ_{ys}^{bm} and σ_{ys}^{wm} denote the yield stress for the base metal and weld metal. The above methodology can then be extended in straightforward manner to define J_p for this crack geometry by the following expression

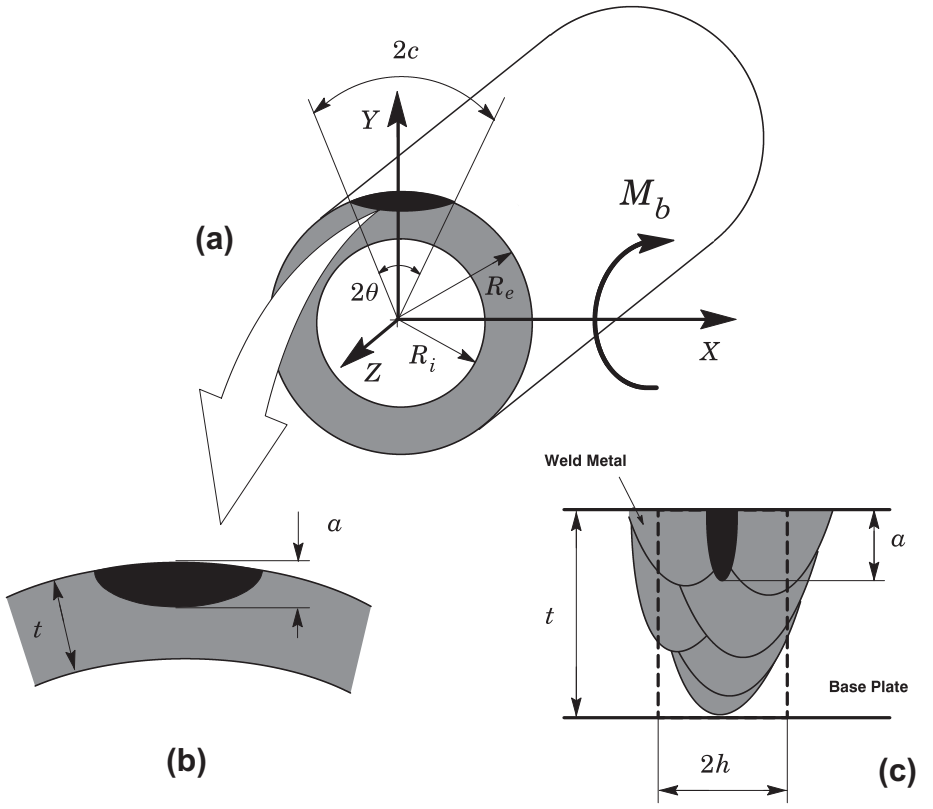

Fig. 1. Circumferentially cracked pipe under bending and weld centerline defect geometry.

$$J_p = \alpha_{wm}\epsilon_{ys}^{wm}\sigma_{ys}^{wm} b\left[h_1\left(\frac{a}{t},\ \frac{D_e}{t},\ \theta,\ \frac{2h}{t},\ M_y,\ n_{wm}\right)\right]\left(\frac{M_b}{M_0^{wm}}\right)^{n_{wm}+1} \tag{6}$$

in which the subscript (superscript) *wm* indicates that the corresponding quantities are related to the weld metal properties. In the above expression, D_e is the pipe (cylinder) outer diameter, t is the wall thickness, $b = t - a$ now defines the uncracked ligament, h is the weld groove half width, M_b denotes the applied bending moment and the surface crack length is described by the angle θ (see Fig. 1) as [13,30]

$$\theta = \frac{\pi c}{2D_e} \tag{7}$$

where c is the circumferential crack half-length.

In the above Eq. (6), the limit bending moment, M_0^{wm}, is defined in terms of the weld material (rather than the base plate material) and conventionally given by [13,30]

$$M_0^{wm} = 2\sigma_{ys}^{wm} R_m^2 t\left(2sin\beta - \frac{a}{t}sin\theta\right) \tag{8}$$

in which R_m denotes the mean radius ($R_m = (R_e + R_i)/2$ where R_e and R_i are the external and internal radius) and parameter β is defined as

$$\beta = \frac{\pi}{2}\left[1 - \left(\frac{\theta}{\pi}\right)\left(\frac{a}{t}\right)\right]. \tag{9}$$

The limit load solution for the bending moment given by Eq. (8) is applicable in the range $(\theta + \beta) \leqslant \pi$ [13,30]. Here, it is also understood that the previous Eq. (8) has a clear interpretation as corresponding to a limit load solution applicable to a circumferentially surface cracked pipe made of a homogeneous material having the weld metal flow properties (yield stress, σ_{ys}^{wm}, and the associated strain hardening exponent, n_{wm}); a condition often referred to as "all weld metal" (AWM).

Finally, the elastic term, J_e, is calculated by using Eq. (2) coupled with a convenient form for the elastic stress intensity factor, K_I. For a circumferential surface crack in a pipe subjected to a (pure) bending moment, an improved expression for parameter K_I is given by API 579 [13] as

$$K_I = \sigma_b G_5 \sqrt{\frac{\pi a}{Q_s}} \tag{10}$$

where σ_b is the (global or net-section) bending stress about the X-axis (see Fig. 1) expressed by

$$\sigma_b = \frac{4M_b R_e}{\pi\left(R_e^4 - R_i^4\right)} \tag{11}$$

with the flaw shape parameter, Q_s, defined as

$$Q_s = 1 + 1.464\left(\frac{a}{c}\right)^{1.65}, \quad a \leqslant c. \tag{12}$$

In the above expression (10), G_5 is the influence coefficient corresponding to a circumferential semi-elliptical surface crack in a cylinder subjected to a (pure) net-section bending as given in Appendix C of API 579 [13].

Evaluation of the applied bending moment, M_b, entering into Eq. (6) deserves further consideration in the particular case of reeling installation. Here, the maximum bending strain in the reeled pipe, ϵ_r, can be calculated directly from the pipe and reel dimensions through the following expression

$$\epsilon_r = \frac{D_e/2}{D_e/2 + R} \tag{13}$$

where D_e is the pipe outer diameter and R denotes the reel radius. While the above expression is directly applicable in strain/displacement controlled defect assessment procedures, it can be also employed to estimate the maximum bending moment in stress-based approaches through the moment-strain relationship for the analyzed pipe configuration. Following Ostby et al. [31] and Chiodo and Ruggieri [25], the moment-strain trajectories for cracked pipes are essentially similar to the corresponding trajectory for an uncracked pipe. Thus, the applied bending moment, M_b, entering into the previous Eq. (6) can be extracted from a moment-strain relationship determined from a routine finite element analysis of the unflawed pipe (see Chiodo and Ruggieri [25]).

3. The reference stress approach

3.1. Approximate representation of fully-plastic J

Another procedure to evaluate the J-integral, which shares much in common with the previous methodology, is essentially a modification of the GE-EPRI approach proposed by Ainsworth [32] to reflect more closely the flow behavior of elastic–plastic materials, particularly high hardening materials such as austenitic stainless steels. This procedure, most often referred to as the reference stress approach, enables evaluation of J by using available stress intensity factor solutions for the cracked component in connection with the adoption of parameter h_1 defined for a linear material in which the strain hardening exponent is set as $n = 1$.

The procedure begins by defining a references stress, σ_{ref}, in the form

$$\sigma_{ref} = \sigma_{ys}\left(\frac{P}{P_0}\right) \tag{14}$$

so that Eq. (4) becomes

$$J_p = b[h_1(a/W,\ \ell,\ n)]\sigma_{ref}\left(\epsilon_{ref} - \sigma_{ref}\frac{\epsilon_{ys}}{\sigma_{ys}}\right) \tag{15}$$

in which ϵ_{ref} is the (uniaxial) reference strain corresponding to σ_{ref} when previous Eq. (3) is invoked to describe the material stress–strain behavior.

By noting that h_1 is relatively insensitive to n, particularly for high hardening materials (lower n-values), Ainsworth [32] proposed the approximation $h_1(n) \approx h_1(n = 1)$ and manipulated Eq. (15) to the form

$$J_p = \frac{\mu K_I^2}{E}\left(\frac{E\epsilon_{ref}}{\sigma_{ref}} - 1\right) \tag{16}$$

where $\mu = 0.75$ or $\mu = 1.0$ corresponds to whether plane-strain or plane-stress conditions are adopted. The above Eq. (16) provides a good approximation for the plastic component of the J-integral in a cracked component, including a circumferentially surface cracked pipe, once a stress-intensity factor solution and stress–strain data for the material are available.

3.2. Extension to include effects of weld strength mismatch

To incorporate the potentially strong effects of weld strength mismatch on the crack driving forces in welded components, Lei and Ainsworth [33,34] proposed to treat the mechanical response of an idealized bimaterial welded joint (*i.e.*,

consisting of the weld and base plate material) in terms of an equivalent stress–plastic strain relationship (ESSR) that approximately describes the coupling influence of the weld geometry and strength mismatch between the weld and base plate material on J. Here, the bimaterial structure is viewed as a homogenous material in which the flow properties are simply described by the weighted mechanical response derived from the stress–strain behavior for the weld and base plate materials.

By considering a convenient limit load analysis of the idealized bimaterial welded joint, the stress-plastic strain response of the equivalent material is defined as [12,33,34]

$$\tilde{\sigma}(\epsilon_p) = \left[\frac{P_0^{Mism} - P_0^{bm}}{P_0^{wm} - P_0^{bm}}\right]\sigma^{wm}(\epsilon_p) + \left[\frac{P_0^{wm} - P_0^{Mism}}{P_0^{wm} - P_0^{bm}}\right]\sigma^{bm}(\epsilon_p) \tag{17}$$

where $\tilde{\sigma}$ is the equivalent (true) stress corresponding to the plastic (true) strain, ϵ_p, level, P_0^{Mism} denotes the limit load of the idealized bimaterial welded joint, and P_0^{bm} and P_0^{wm} represent the limit load for the homogeneous component made of the base plate material and weld metal. In the above expression, it is also understood that $\sigma^{bm}(\epsilon_p)$ and $\sigma^{wm}(\epsilon_p)$ are the (true) stress corresponding to the plastic (true) strain level, ϵ_p, for the base plate material and weld metal. The equivalent stress–plastic strain relationship defined by Eq. (17) is then used in conjunction with previous Eq. (16) to determine an improved estimate of J_p for the idealized bimaterial welded joint, rather than the homogeneous component made either of the base plate material or the weld metal. The methodology described by Eq. (17) is also included in Level 3 of the SINTAP procedure [12], in the R6 procedure [35] and in the recent revision of BS 7910 [11].

Evaluation of the equivalent stress-plastic strain response based on the ESSR procedure outlined above requires specification of a proper limit load solution for the idealized bimaterial welded joint once all other quantities entering directly into the calculation of $\tilde{\sigma}(\epsilon_p)$ are defined. While a number of limit load solutions covering a wide range of geometries and crack configurations are available, there is unfortunately no specific limit load solution for a circumferentially surface crack in the girth weld of a pipe or cylinder under bend loading. However, we can advantageously evaluate Eq. (17) for the problem addressed here based on an approximate limit load solution of a plate containing a weld centerline, surface crack given by Song et al. [36]. Section 7 provides the critical flaw sizes for an undermatching girth weld of a typical clad pipe employed in subsea flowlines based on the reference stress approach defined by Eq. (16) using Eq. (17) to describe the equivalent stress–plastic strain response for the girth weld.

4. FAD-based defect assessment methodologies

4.1. Fundamental FAD assessment curve

ECA procedures of crack-like defects based upon the FAD philosophy have undergone extensive developments in the past decade to form the basis for industrial codes and guidelines for structural integrity assessments. A fundamental approach, derived from the early work by Dowling and Townley [37] and Harrison et al. [38], to address the potential interaction between brittle fracture and plastic collapse adopts the concept of a two-criteria failure assessment diagram to describe the mechanical integrity of flawed components schematically illustrated in Fig. 2. Here, a geometry and material independent failure line is constructed based upon a relationship between the normalized crack-tip loading, K_r, and the normalized applied (remote) loading, L_r, in the form

$$K_r = \left[1 - 0.14(L_r)^2\right]\left\{0.3 + 0.7\exp\left[-0.65(L_r)^6\right]\right\} \tag{18}$$

for $L_r \leqslant L_r^{max}$ in which the cut-off parameter, L_r^{max}, is most often given by

$$L_r^{max} = \frac{1}{2}\left(1 + \frac{\sigma_{uts}}{\sigma_{ys}}\right) \tag{19}$$

where σ_{ys} and σ_{uts} are the material's yield stress and tensile strength. Further, ECA procedures more applicable to submarine pipelines, such as DNV F101 [39], also define the cut-off parameter, L_r^{max}, simply as

$$L_r^{max} = \frac{\sigma_{uts}}{\sigma_{ys}}. \tag{20}$$

In the above expression (18), the toughness ratio, K_r, and the load ratio, L_r, are simply defined as

$$K_r = \frac{K_I}{K_{mat}} \tag{21}$$

and

$$L_r = \frac{\sigma_{ref}}{\sigma_{ys}} \tag{22}$$

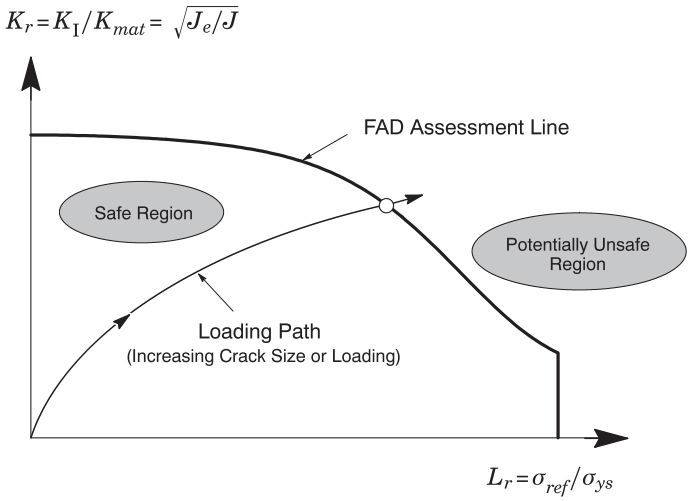

Fig. 2. Schematic illustration of the FAD methodology.

where K_I is the (Mode I) elastic stress intensity factor, K_{mat} denotes the material's fracture toughness and the reference stress, σ_{ref}, characterizes the plastic collapse load for the cracked component. Current defect assessment procedures based on Eq. (18) include BS7910 Level 2A [11] and API 579 Level 2 [13] procedures which have arguably emerged as the engineering codes most widely used in integrity assessments of structural components containing crack-like flaws. Structural integrity assessments of a cracked component is based on the relative location of the assessment point with respect to the FAD curve defined by each procedure (see Fig. 2). The component is simply considered safe if the assessment point lies below the FAD line whereas it is considered potentially unsafe if the assessment point lies on or above the FAD curve. An increased load or larger crack will move the assessment point along the loading path towards the failure line.

4.2. Material dependent FAD curve

A key feature of the FAD methodology previously described lies in the adoption of a geometry independent failure line to provide a single failure locus applicable in general integrity assessments. When the approximation of geometry and material independence of the FAD curve described by Eq. (18) becomes inappropriate, additional modifications are necessary to provide a more useful approach. In general, a proper definition of L_r, as described in Anderson [9], is effective to remove the geometry dependence of the FAD curve.

To introduce a material dependent FAD curve, Milne et al. [40] further generalized the reference stress approach outlined previously to include a material specific dependence of the toughness ratio, K_r, on load ratio, L_r, defined by

$$K_r = \left[\frac{E\epsilon_{ref}}{L_r\sigma_{ys}} + \frac{L_r^3\sigma_{ys}}{2E\epsilon_{ref}}\right]^{-1/2} \tag{23}$$

where E is the longitudinal elastic modulus, ϵ_{ref} represents the reference strain and $L_r = \sigma_{ref}/\sigma_{ys}$ with σ_{ref} denoting the reference stress. Eq. (23) yields generally more accurate assessments of cracked components when compared with previous Eq. (18) while, at the same time, allowing the consideration of the full stress–strain data, including materials exhibiting a yield discontinuity (Lüders plateau [29]). Further, the above Eq. (23) is also included in BS7910 [11] as Level 2B and API 579 [13] as Level 3B.

The above methodology cast into the form of Eq. (23) can be extended in straightforward manner to include the effects of weld strength mismatch on the dependence of the toughness ratio, K_r, on load ratio, L_r, upon replacing the material yield stress, σ_{ys}, by the weld metal yield stress, σ_{ys}^{wm}. However, while the procedure provides conservative assessments in the case of undermatched welds for which $M_y < 1$, it may potentially lead to non-conservative assessment results for overmatched welds for which $M_y > 1$. Thus, use of the yield stress of the base metal or base plate material, σ_{ys}^{bm}, in previous Eq. (23) may be strongly advisable for practical assessments of overmatched welded components, where adequate levels of conservatism are needed.

4.3. Advanced FAD assessment methods including weld strength mismatch

While the previous FAD-based methodology described by Eq. (18) proves sufficiently effective to define defect acceptance criteria for homogeneous materials, it is not necessarily applicable in this standard form to assess the significance of

structural defects in welded components with weld metal strength mismatch. As already mentioned, mismatch in the flow properties between the weld metal and the base plate material alters the coupling relationship between remote loading and crack-tip loading (as characterized by J or CTOD) while, at the same time, also affecting the plastic collapse load of the cracked welded component.

A more advanced FAD formulation including the effects of weld metal strength mismatch can be derived by defining the toughness ratio as

$$K_r = \sqrt{\frac{J_e}{J}} \tag{24}$$

where J is the total value of the applied J-integral and J_e represents its elastic component. Now, by making use of the connection between J and K and following API 579 [13] to define the reference stress, σ_{ref},

$$\sigma_{ref} = \frac{M_b}{2R_m^2 t\left(2sin\beta - \frac{a}{t}sin\theta\right)} \tag{25}$$

an improved form of toughness ratio, K_r, yields

$$K_r = \sqrt{\frac{J_e}{J_e + J_p}} = \sqrt{\left[1 + \frac{H_{wm}}{J_e}\left(L_r^{wm}\right)^{n_{wm}+1}\right]^{-1}} \tag{26}$$

in which the fully plastic solution to describe J_p is given by previous Eq. (6) with H_{wm} then written as

$$H_{wm} = \alpha_{wm}\epsilon_{ys}^{wm}\sigma_{ys}^{wm} b\left[h_1(a/t,\ D_e/t,\ \theta,\ 2h/t,\ M_y,\ n_{wm})\right]. \tag{27}$$

and the load ratio, L_r^{wm}, defined by previous Eq. (22) with the material yield stress replaced by the yield stress of the weld metal.

A key feature of the above methodology is that it derives entirely from elastic–plastic J solutions based upon detailed finite element analyses thereby incorporating virtually any geometry and material dependence in the FAD procedure. Subsequent section will address an application of this advanced FAD formulation including the effects of weld metal strength mismatch to assess critical flaw sizes for a CRA clad pipe with an undermatch girth weld.

5. Numerical procedures and material models

5.1. Finite element models for pipeline girth welds with weld centerline cracks

Nonlinear 3-D finite element analyses are conducted on pipeline girth welds with external, circumferential surface flaws at weld centerline subjected to bending. The analyzed pipe models have wall thickness $t = 20.6$ mm with different outside diameters: $D_e = 206$ mm ($D_e/t = 10$); $D_e = 309$ mm ($D_e/t = 15$) and $D_e = 412$ mm ($D_e/t = 20$). These geometries typify current trends in high pressure, high strength pipelines, including submarine pipelines and risers. The pipeline girth weld is modeled as a bimaterial system (the commonly narrow heat affected zone – HAZ – is not considered in the present work) with a square groove having width $2h = 15$ mm ($h/t = 0.36$). The analysis matrix considers weld centerline surface flaws with varying crack depth, a, and different crack length, $2c$, as defined by a/t = 0.1–0.4 with increments of 0.1 and $\theta/\pi = 0.04$, 0.12 and 0.20 – refer to Eq. (7) and Fig. 1 for the crack geometry definition. Overall, the computations comprised 36 numerical models in 3-D and 324 loading cases considering the several hardening levels for the weld metal adopted in the analyses.

The modeling of the girth weld geometry deserves further attention. While the weld groove width may affect the computed h_1-factors, the present investigation employs a square groove weld having $2h = 15$ mm ($h/t = 0.36$), which corresponds to an average weld profile for typical welding procedures applicable to oil and gas pipelines. Recent work conducted by Paredes and Ruggieri [41] demonstrates a relatively weak effect of the weld groove width on factor h_1 for mismatched welds in the range of $\pm 20\%$ ($M_y = 1.2$ and $M_y = 0.8$ – refer to Eq. (5)). Consequently, the present results appear sufficiently applicable to determine the J-integral in dissimilar pipe girth welds with slightly distinct h/t-ratios, as will be addressed later.

Fig. 3 shows the finite element model constructed for the pipe with $D_e/t = 10$, $a/t = 0.2$ and $\theta/\pi = 0.12$. A conventional mesh configuration having a focused ring of elements surrounding the crack front is used with a small key-hole geometry (blunt tip) at the crack tip to enhance numerical convergence and to accommodate the large plastic strains that develop with increased levels of deformation. The small initial root radius at the crack tip is $\rho_0 = 0.001$ mm. A typical half-symmetric model for the cracked pipes has approximately 15,000 elements and 18,000 nodes with appropriate constraints imposed on nodes defining the symmetry planes. The crack front is described by 15 (circumferential) layers defined over the crack half-length (c); the thickest layer is defined at the deepest point of the crack with thinner layers defined near the free surface to accommodate the strong gradient in the stress distribution along the crack front. The half-symmetric finite element models for the pipe specimens are loaded by a four-point bending scheme so that a constant bending moment with zero

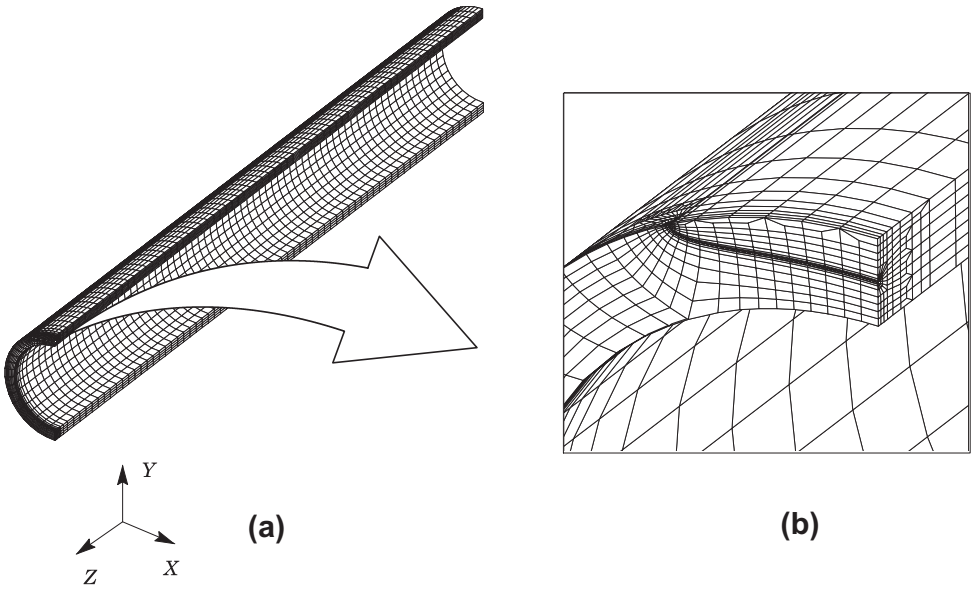

Fig. 3. Typical finite element model for the analyzed circumferentially cracked pipe with $D_e/t = 10$, having an external surface flaw with $a/t = 0.2$ and $\theta/\pi = 0.12$ at girth weld centerline.

shear forces is imposed on the crack plane and along the pipe half-length at distances about three times the pipe diameter. Exploratory numerical analyses demonstrate that such loading scheme and associated boundary conditions, including the adopted pipe length, does not influence the near-tip stress and strain fields nor does it affect the J-values extracted from the finite element computations. Very similar finite element models and mesh details are employed for other cracked pipe configurations.

5.2. Material models and finite element procedures

The elastic–plastic constitutive model employed in all analyses reported here follows a flow theory with conventional Mises plasticity in small geometry change (SGC) setting. The numerical solutions for the cracked pipes utilize a simple power-hardening model to characterize the uniaxial true stress ($\bar{\sigma}$) vs. logarithmic strain ($\bar{\epsilon}$) in the form

$$\frac{\bar{\epsilon}}{\epsilon_{ys}} = \frac{\bar{\sigma}}{\sigma_{ys}}\ ,\ \epsilon \leqslant \epsilon_{ys};\ \frac{\bar{\epsilon}}{\epsilon_{ys}} = \left(\frac{\bar{\sigma}}{\sigma_{ys}}\right)^{n},\ \epsilon > \epsilon_{ys} \tag{28}$$

where σ_{ys} and ϵ_{ys} are the reference (yield) stress and strain, and n is the strain hardening exponent. The finite element analyses consider material flow properties covering a typical range of weld metal strength mismatch levels: 20% undermatch, evenmatch and 25% overmatch ($M_y = 0.8$, 1.0 and 1.25 – see Eq. (5) defining the mismatch ratio). The following yield stress and strain hardening properties of the base plate material are assigned in all analyses: $\sigma_{ys} = 483$ MPa and $n = 12$ which

Table 1
Material properties adopted in the analyses of the pipeline girth welds with weld centerline cracks.

Mismatch level	Weld metal		Base plate	
	σ_{ys} (MPa)	n	σ_{ys} (MPa)	n
20% Undermatch	386	6	483	12
		8		
		10		
		12		
25% Overmatch	604	12	483	12
		14		
		16		
		18		
Evenmatch	483	12	483	12

typify an API X60 pipeline grade steel; Chiodo and Ruggieri [25] utilized these material properties in their analyses of circumferentially cracked pipes subjected to reeling.

Table 1 provides the material properties utilized in the numerical analyses of the pipeline girth welds which also consider E = 206 GPa and ν = 0.3. Because the actual flow properties of weld metal depend on a number of key factors including the welding process, heat input and type of weld consumable among others, the strain hardening exponents for the weld metal are varied such as to cover a realistic range of strain hardening behavior (higher hardening to lower hardening for a fixed weld metal yield stress). In particular, the 20% undermatch weld metal ($\sigma_{ys}^{wm} = 386$ MPa) with $n = 6$ material (high hardening behavior) typifies a partially undermatching condition commonly observed in girth welds of CRA clad pipes; here, at a certain (plastic) deformation level, the weld metal actually overmatches the base plate material.

The finite element code WARP3D [42] provides the numerical solutions for the computational analyses reported here. The code formulates and solves the equilibrium equations at each iteration using parallel algorithms and implements the so-called $\overline{\mathbf{B}}$ formulation (see [42] for details) to preclude mesh lock-ups that arise as the deformation progresses into fully plastic, incompressible modes. The local value of the mechanical energy release rate at a point along the crack front is given by [43]

$$J = \lim_{\Gamma \to 0} \int_{\Gamma} \left[W_s n_1 - \sigma_{ij} \frac{\partial u_i}{\partial x_1} n_j \right] d\Gamma \tag{29}$$

where Γ denotes a contour defined in a plane normal to the front on the undeformed configuration beginning at the bottom crack face and ending on the top face, n_j is the outward normal to Γ, W_s denotes the stress-work density per unit of undeformed volume, σ_{ij} and u_i are Cartesian components of stress and displacement in the crack front coordinate system. The finite element computations employ a domain integral procedure [43] for numerical evaluation of Eq. (29) to provide pointwise and front average values of J across the crack front at each loading level. For the 3-D analyses of the circumferentially surface cracked pipes, the intensity of near-tip deformation is quantified by the pointwise value of J evaluated at the point of maximum crack depth (see Fig. 3). Because the near-tip stress triaxiality is maintained over a large portion of the crack front at the deepest point region and at distances sufficiently far from the traction-free (external) face of the pipe [44], this J-value adequately characterizes the level of crack-tip loading level needed in the estimation procedure for parameter h_1 conducted next. The research code FRACTUS2D [45] is employed to compute the h_1-factors for the analyzed circumferentially cracked pipes with weld centerline cracks.

5.3. Numerical modeling and mesh refinement issues

We briefly comment on those computational details that have a direct bearing on the evaluation of the J-integral for the girth welds with external, circumferential surface flaws at weld centerline subjected to bending. Since factor h_1 derives directly using the relation between J_p and applied bending moment, M_b, defined by Eq. (6), potential deviations in the computed J-values are reflected in the computation of the h_1-factors as well.

In the present computational framework, a requisite feature to obtain adequate numerical descriptions of the crack-tip stress and strain fields which are accurate over distances of order a few CTODs and, at the same time, provide path-independent J-values at distances sufficiently far from the crack tip is the use of a highly refined near-tip mesh of numerically efficient 8-node, 3-D elements (see details of the element formulation in [42]). A weak, implicit length-scale enters the finite element computations through the near-tip mesh size as insufficient mesh refinement reduces the stress values ahead of the crack front, especially at smaller load levels. However, the 3-D models used in this study possess the required level of mesh refinement to resolve accurately the crack-tip stresses and deformation fields to minimize any mesh dependencies of the computed J-values.

To demonstrate the adequacy of the near-tip mesh refinement used in the present study, consider first the variation of the computed J-integral, denoted as J_{domain}, from several annular domains, as characterized by increased domain radius, r_{domain}, normalized by the weld groove half-width, h, with varying blunt notch radius, $\rho_0 = 0.001$, 0.005 and 0.01 mm, for the pipe model with $D_e/t = 15$, $a/t = 0.2$ and 0.4, $\theta/\pi = 0.12$ and different strength mismatch levels depicted in Fig. 4(a–d). Here, the domain radius, r_{domain}, is simply defined by the near-tip distance at which the annular domain intercepts the X-axis at $Z = 0$. For the present discussion, the load level is taken as the applied (remote) load corresponding to the value of $J \approx 400$ kJ/m^2, which approximately defines the onset of ductile tearing reported in previous crack growth resistance testing for Alloy 625 materials as noted later in Section 7.1.

For the annular domains close to the crack tip, in which strong nonproportional loading and intense plastic strain effects prevail, the computed J-values are higher but fall drastically as the nondimensional radius is sufficiently far from the crack tip. After this transitional behavior, the computed J-integral is essentially independent of the adopted contour integration along paths remote from the crack tip and inside the weld groove thereby providing virtually path-independent J-values. Further, also observe that the path-independent J-values are weakly sensitive to the blunt notch radius, ρ_0, for all analyzed crack configurations and strength mismatch levels. In particular, there are essentially no differences between the computed J-values for the numerical models with $\rho_0 = 0.001$ and 0.005 mm (recall that the present numerical analyses employ $\rho_0 = 0.001$ mm). Essentially similar results are obtained for other pipe configurations and strength mismatch levels but are not shown here in interest of space. Moreover, we also note that the computed J-values are in close agreement with

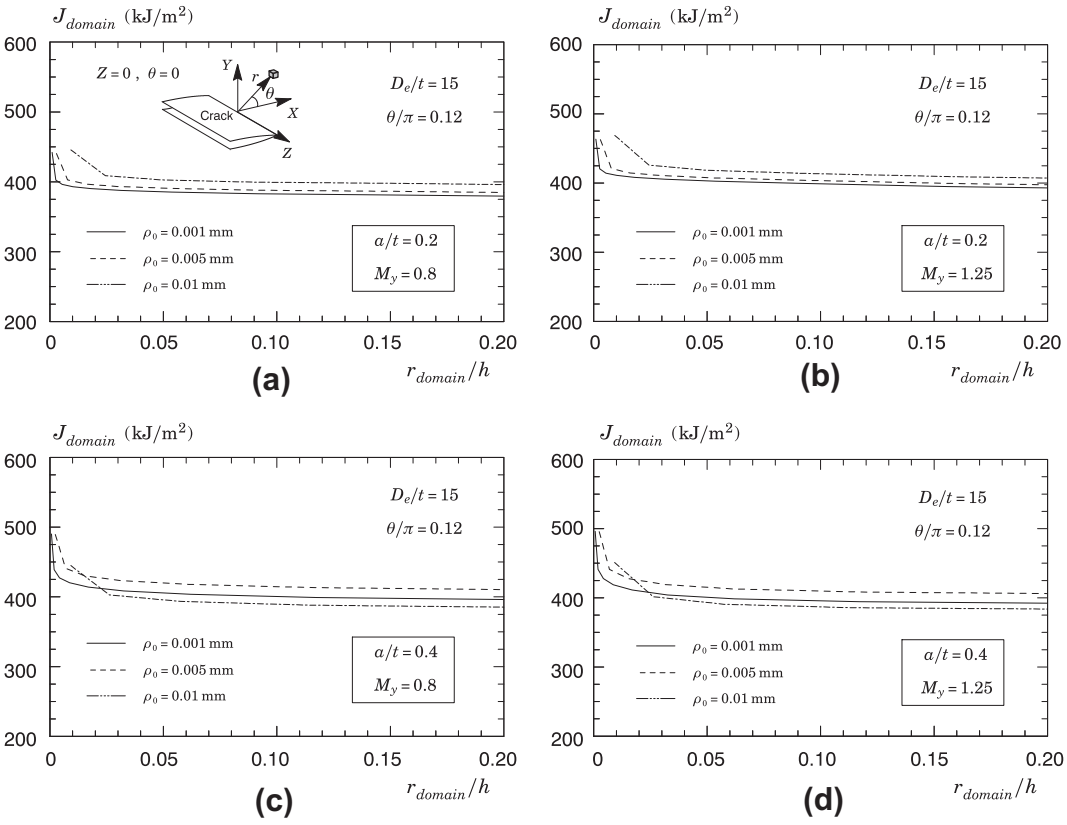

Fig. 4. Variation of the computed J-integral from several annular domains with varying blunt notch radius for the pipe model with $D_e/t = 15$, $\theta/\pi = 0.12$ and different strength mismatch levels: (a and b) $a/t = 0.2$; (c and d) $a/t = 0.4$.

the corresponding K-values under small scale yielding (SSY) conditions as long as the radii of the annular domains are sufficiently large compared to the distance over which strong nonproportional loading and intense plastic strain effects prevail.

Consider next the evolution of J with applied bending moment, M_b, and varying blunt notch radius, $\rho_0 = 0.001$, 0.005 and 0.01 mm, again for the pipe model with $D_e/t = 15$, $a/t = 0.2$ and 0.4, $\theta/\pi = 0.12$ and different strength mismatch levels illustrated in Fig. 5(a–d). In these plots, the bending moment is normalized by the limit bending moment, M_0^{wm}, corresponding to each analyzed case. The trends are clear. The $J - M_b$ curves for every ρ_0 considered are virtually indistinguishable from each other for the entire range of applied load. The results displayed in Fig. 5 convincingly demonstrate the adequacy of the finite element modeling and mesh refinement used in the present investigation. Again, very similar results are obtained for other pipe configurations and strength mismatch levels – to conserve space, they are not shown here.

6. Factors h_1 for girth welds with weld centerline surface cracks

6.1. Evaluation procedure of h_1-factors for pipe girth welds with circumferential cracks

Before proceeding with evaluation of factor h_1 for the girth-welded, circumferentially cracked pipes analyzed here, the numerical procedure to determine the h-factors is briefly presented. Evaluation of these parameters for the analyzed crack configurations is based on solving Eq. (6) using the computed values for the plastic component of the J integral, J_p, with the applied bending moment, M_b, for a given crack size, component geometry and degree of weld strength mismatch, M_y (which also includes effects of the material strain hardening capacity). The procedure to determine the dimensionless function h_1 simply derives from rewriting Eq. (6) as

$$\bar{J}_p = \frac{J_p}{\alpha \epsilon_{ys}^{wm} \sigma_{ys}^{wm} b} = h_1\left(a/t, D_e/t, \theta, M_y, n_{wm}\right)\left(\frac{M_b}{M_0^{wm}}\right)^{n_{wm}+1} \tag{30}$$

from which factor h_1 is obtained by computing the slope of a least square fit to the variation of $\bar{J}_p$ with $\left(M_b/M_0^{wm}\right)^{n_{wm}+1}$. The estimation procedure developed by Chiodo and Ruggieri [25] is adopted here to evaluate the h_1-factors using the following strategy: (1) determine the J_p-value corresponding to the limit bending moment evaluated from Eq. (6) using the yield stress

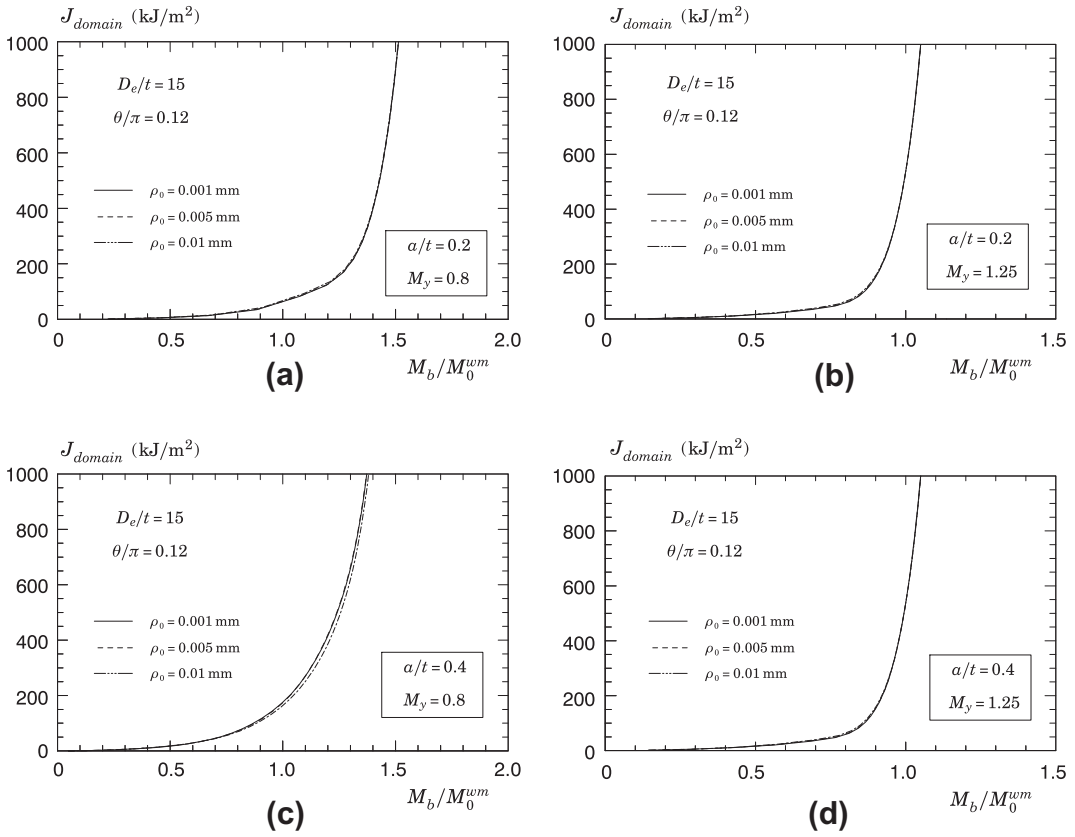

Fig. 5. Evolution of J with applied bending moment, M_b, and varying blunt notch radius for the pipe model with $D_e/t = 15$, $\theta/\pi = 0.12$ and different strength mismatch levels: (a and b) $a/t = 0.2$; (c and d) $a/t = 0.4$.

for the weld metal, σ_{ys}^{wm}; let J_{p-y}^{wm} denote this crack-tip loading level; (2) determine the J_p-value corresponding to the limit bending moment evaluated from Eq. (6) but with the yield stress, σ_{ys}, replaced by the (ultimate) tensile stress, σ_{uts}^{wm}, for the weld metal; let J_{p-t}^{wm} denote this crack-tip loading level; (3) for the J_p-values ranging from J_{p-y}^{wm} to J_{p-t}^{wm}, plot $J_p^{wm}/(\alpha_{wm}\epsilon_0^{wm}\sigma_0^{wm}b)$ vs. $(M_b/M_0^{wm})^{n_{wm}+1}$ and evaluate the h_1 factor as the slope of the best fit straight line passing through the axis origin for the selected range of crack-tip loading. The above strategy maintains consistency with the linear relationship condition between $J_p^{wm}/(\alpha_{wm}\epsilon_0^{wm}\sigma_0^{wm}b)$ and $(M_b/M_0^{wm})^{n_{wm}+1}$ while avoiding considering unrealistically high levels of crack-tip loading (as characterized by J-values larger than J_{p-t}^{wm}) which would otherwise enter into the linear fitting scheme. Readers are referred to Chiodo and Ruggieri [25] for further details on the adopted h_1 estimation scheme.

To illustrate the ability of the adopted estimation procedure in providing consistent h_1-values, Fig. 6 provides the evolution of $\bar{J}_p$ with $(M_b/M_0)^{n_{wm}+1}$ for selected girth-welded, cracked pipe geometries with varying crack sizes and mismatch levels. These analyses include the pipe model with $D_e/t = 15$, $a/t = 0.2$ and 0.4, $\theta/\pi = 0.12$ and different strength mismatch levels: $M_y = 0.8$ and 1.25 (see Eq. (5)), including varying strain hardening exponents for the weld metal, n_{wm}. Neglecting a short transient region, which corresponds to applied load levels (here characterized by the bending moment) that are not essentially relevant in describing fully plastic stress states, a linear relationship between $\bar{J}_p$ and $(M_b/M_0^{wm})^{n_{wm}+1}$ clearly holds true for the entire range of load level for all analyzed cases covering widely different weld metal flow properties, as characterized by the yield stress and hardening exponent of the weld metal. Here, the slope of the straight line derived from the best fit to the computed values of $\bar{J}_p$ with $(M_b/M_0)^{n_{wm}+1}$ as indicated in the plots shown in Fig. 6 unambiguously defines factor h_1 for the analyzed crack configurations. Essentially similar trends and results are obtained for other pipe configurations, including different values of a/t and θ/π, but are again not shown here in interest of space.

6.2. Dependence of factor h_1 on crack geometry and mismatch level

Figs. 7–9 provide the h_1-factors for the pipeline girth welds with weld centerline cracks and varying geometries and strength mismatch levels derived from the J estimation procedure just outlined. For all sets of analyses, the results reveal

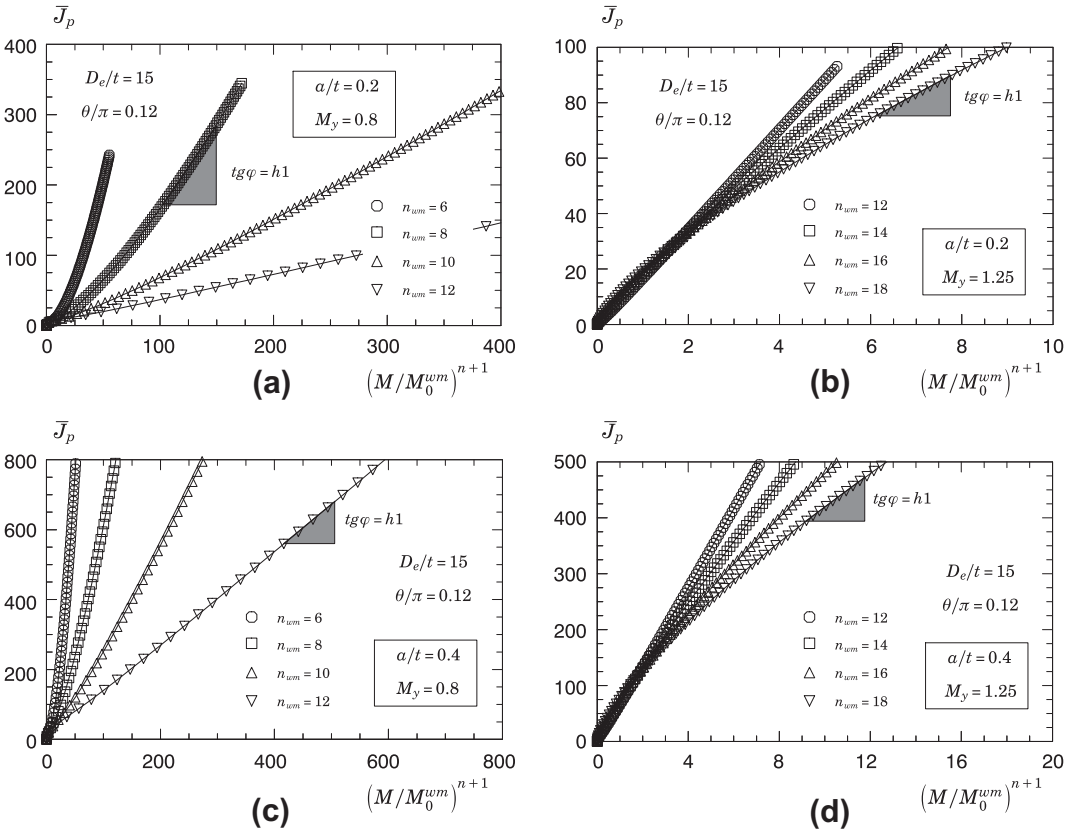

Fig. 6. Evolution of $\bar{J}_p$ with $(M/M_0)^{n+1}$ for the pipe model with $D_e/t = 15$, $a/t = 0.2$ and 0.4, $\theta/\pi = 0.12$ and varying mismatch levels: (a and b) $a/t = 0.2$; (c and d) $a/t = 0.4$.

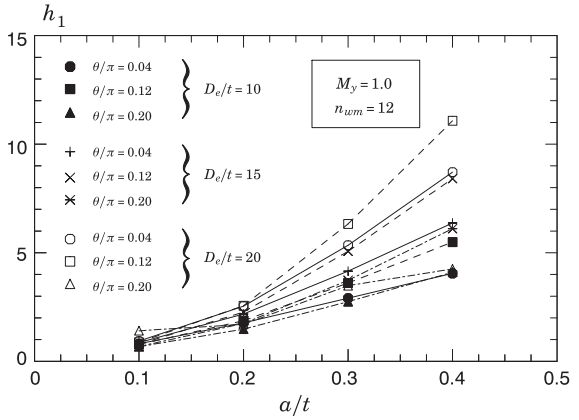

Fig. 7. Variation of factor h_1 with a/t-ratio for the evenmatch pipe girth weld ($M_y = 1.0$) and different D_e/t and θ/π ($n_{wm} = 12$).

that factor h_1 displays a rather strong sensitivity to crack geometry and mismatch level as described the a/t-ratio and M_y-values. Consider first the 20% undermatch ($M_y = 0.8$) results shown in Fig. 8. The significant features include: (1) the h_1-factors display strong sensitivity to the adopted strain hardening exponent for the weld metal; (2) factors h_1 exhibit a relatively strong dependence on the D_e/t-ratio and crack length (as characterized by θ/π) for moderate to deep crack sizes ($0.25 \leqslant a/t \leq 0.4$) and (3) factors h_1 are almost insensitive to the D_e/t-ratio and θ/π-ratio in the shallow crack size range ($0.1 \leqslant a/t \leq 0.2$). Consider now the evenmatch ($M_y = 1.0$) and 25% overmatch ($M_y = 1.25$) results shown in Figs. 7 and 9. The overall trends remain similar with the exception that the h_1-factors now display less sensitivity to the strain hardening exponent of the weld metal for the analyses with 25% overmatch.

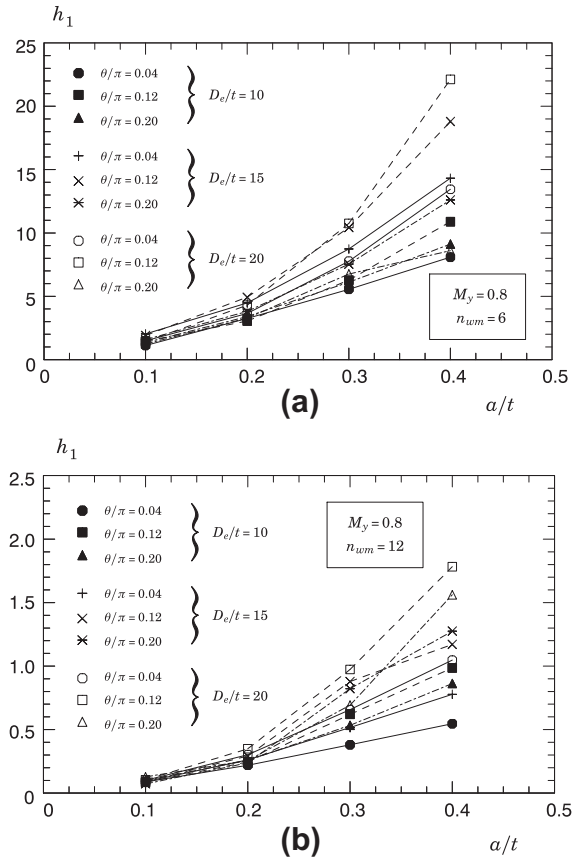

Fig. 8. Variation of factor h_1 with a/t-ratio for the pipe girth weld with 20% undermatch ($M_y = 0.8$) and different D_e/t and θ/π: (a) $n_{wm} = 6$; (b) $n_{wm} = 12$.

To provide a simpler manipulation of the previous results aiming at developing ECA procedures applicable to structural integrity assessments of pipeline girth welds with circumferential surface cracks subjected to bending, a functional dependence of factor h_1 on crack geometry (as characterized by a/t and θ/π) for a given D_e/t-ratio and mismatch level, M_y, including the strain hardening exponent for the weld metal, is constructed in the form

$$h_1 = \xi_0 + f(a/t) + g(\theta/\pi) \tag{31}$$

with

$$f(a/t) = \xi_1(a/t) + \xi_2(a/t)^2 + \xi_3(a/t)^3 \tag{32}$$

and

$$g(\theta/\pi) = \xi_4(\theta/\pi) + \xi_5(\theta/\pi)^2 \tag{33}$$

where a multivariate polynomial fitting is adopted to describe the variation of factor h_1 with crack geometry. A standard least square fitting using the Mathematica software [46] to the computed h_1-factors gives the coefficients presented in Tables 2–4 which are essentially valid in the range $0.1 \leqslant a/t \leq 0.4$ and $0.04 \leqslant \theta/\pi \leq 0.20$.

To illustrate the degree of correlation between the multivariate fitting defined by Eqs. (31)–(33) and the computed h_1-values, Fig. 10 shows the dependence of h_1 on a/t for the pipe model with $D_e/t = 15$ and varying crack lengths, as characterized by θ/π for two widely distinct cases: (1) an undermatched girth weld ($M_y = 0.8$) in which $n_w = 6$ and (2) an overmatched girth weld ($M_y = 1.25$) for which $n_w = 18$. In these plots, the solid symbols represent the computed h_1-values whereas the lines define the curve fitting derived from the above expressions. Given the relative difficulty of performing a multivariate fitting based on a standard least square procedure using only few sampling points (four a/t-values and three θ/π-values), the fitted curves are in good accord with the general trend of computed values - indeed, the larger differences between the fitted and computed values are usually less than 10%. Very similar trends are found for other crack configurations and material properties but are not shown here to conserve space.

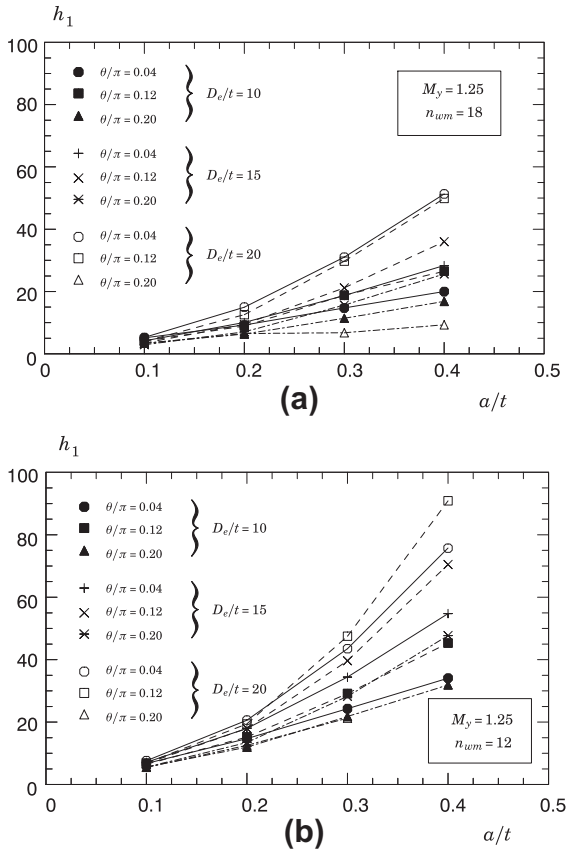

Fig. 9. Variation of factor h_1 with a/t-ratio for the pipe girth weld with 25% overmatch ($M_y = 1.25$) and different D_e/t and θ/π: (a) $n_{wm} = 18$; (b) $n_{wm} = 12$.

Table 2
Coefficients for the polynomial fitting of factor h_1 given by Eqs. (31)–(33) for 20% undermatch girth weld ($M_y = 0.8$) with weld groove width of $h/t = 0.36$ and base plate material having $\sigma_{ys}^{bm} = 483$ MPa and $n_{bm} = 12$ (polynomial fitting valid in the range $10 \leqslant D_e \leq 20$, $0.1 \leqslant a/t \leq 0.4, 0.04 \leqslant \theta/\pi \leq 0.2$ and $6 \leqslant n_{wm} \leq 12$).

D_e/t	n_{wm}	ξ_0	ξ_1	ξ_2	ξ_3	ξ_4	ξ_5
10	6	−1.06	3.79	58.32	−29.00	28.18	−104.59
	8	−0.38	0.96	21.25	−20.38	10.57	−46.20
	10	−0.01	−3.58	26.51	−29.41	5.43	−19.85
	12	−0.11	−2.20	16.35	−17.22	4.96	−17.30
15	6	−1.32	−4.94	105.44	−14.81	73.42	−332.20
	8	−0.71	3.65	11.20	7.87	14.66	−60.63
	10	−0.10	−3.40	26.59	−22.82	7.32	−27.88
	12	0.33	−10.63	58.32	−72.53	5.00	−15.87
20	6	−2.85	−24.59	188.51	−119.96	135.22	−605.58
	8	−0.61	9.15	−22.30	67.49	13.34	−71.91
	10	0.34	−13.99	72.45	−76.15	12.94	−52.40
	12	−0.17	−3.41	20.13	−10.25	8.67	−32.65

7. Tolerable crack size estimates for CRA clad pipes with undermatch girth weld

To demonstrate the effectiveness of the methodology presented previously in advanced defect assessment procedures for cracked structural components, this section examines the prediction of critical flaw sizes for a typical clad pipe employed in subsea flowlines having a girth weld made of UNS N06625 Alloy 625. Conducted as part of a collaborative program between the University of São Paulo and Petrobras (Brazilian State Oil Company), the verification studies conducted here compare estimates of tolerable crack sizes based upon an ECA procedure incorporating the fully plastic solutions described previously

Table 3
Coefficients for the polynomial fitting of factor h_1 given by Eqs. (31)–(33) for 25% overmatch girth weld ($M_y = 1.25$) with weld groove width of $h/t = 0.36$ and base plate material having $\sigma_{ys}^{bm} = 483$ MPa and $n_{bm} = 12$ (polynomial fitting valid in the range $10 \leqslant D_e \leq 20$, $0.1 \leqslant a/t \leq 0.4$, $0.04 \leqslant \theta/\pi \leq 0.2$ and $12 \leqslant n_{wm} \leq 18$).

D_e/t	n_{wm}	ξ_0	ξ_1	ξ_2	ξ_3	ξ_4	ξ_5
10	12	−2.15	−18.70	414.64	−409.11	179.98	−805.60
	14	−0.26	−38.57	451.66	−493.89	161.22	−738.44
	16	0.88	−49.44	461.00	−536.21	143.60	−675.65
	18	2.72	−66.33	489.21	−580.16	121.40	−578.25
15	12	−2.50	−46.29	554.72	−288.37	253.59	−1182.33
	14	−0.21	−42.81	492.30	−343.13	178.44	−871.28
	16	1.17	−43.75	445.45	−351.09	123.43	−616.00
	18	1.22	−55.58	459.64	−408.92	114.72	−543.02
20	12	0.29	−84.67	766.73	−525.16	427.67	−2335.86
	14	1.41	−52.28	578.89	−398.26	349.76	−2021.78
	16	1.62	−8.21	324.36	−122.35	266.12	−1650.52
	18	3.63	−4.28	285.91	−142.36	179.53	−1247.36

Table 4
Coefficients for the polynomial fitting of factor h_1 given by Eqs. (31)–(33) for evenmatch case ($M_y = 1.0$) with $\sigma_{ys}^{bm} = 483$ MPa and $n_{bm} = 12$ base plate material (polynomial fitting valid in the range $10 \leqslant D_e \leq 20$, $0.1 \leqslant a/t \leq 0.4$, $0.04 \leqslant \theta/\pi \leq 0.2$).

D_e/t	ξ_0	ξ_1	ξ_2	ξ_3	ξ_4	ξ_5
10	2.72	−66.33	489.21	−580.16	121.40	−578.25
15	1.22	−55.58	459.64	−408.92	114.72	−543.02
20	3.63	−4.28	285.91	−142.36	179.53	−1247.36

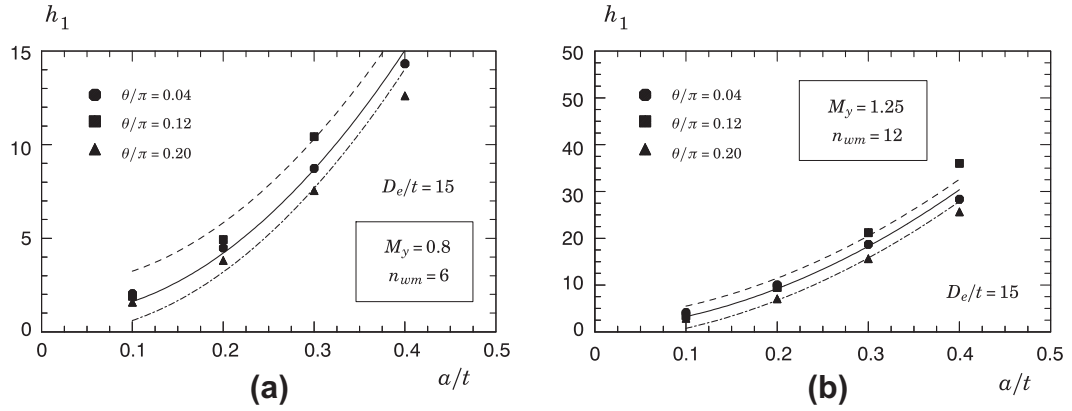

Fig. 10. Dependence of fitted and computed h_1-values on a/t derived from Eqs. (31)–(33) for the pipe model with $D_e/t = 15$ and varying crack lengths, as characterized by θ/π for two widely distinct cases: (a) undermatched girth weld ($M_y = 0.8$) in which $n_w = 6$ and (b) overmatched girth weld ($M_y = 1.25$) for which $n_w = 18$.

with crack size estimates obtained directly from conventional FAD methodologies, including the reference stress approach outlined in Section 4.2 based on the equivalent stress-plastic strain response defined by Eq. (17).

7.1. Pipe geometry and material properties

The verification analyses consider the girth weld for a typical C–Mn pipe internally clad with UNS N06625 Alloy 625 [1,2]. Fig. 11(a) shows the idealized girth weld geometry illustrating the crack depth, a, the steel pipe wall thickness, t_{steel}, and the clad liner thickness, t_{CRA}. Experimental work conducted by Hippert [47] shows that a typical macro section of the CRA girth weld clearly reveals the dissimilar character of weld metal in sharp contrast with the base plate material. The analyzed pipe has outside diameter, $D_e = 203.2$ mm (8 in), steel pipe thickness, $t_{steel} = 15$ mm and clad liner thickness, $t_{CRA} = 5$ mm thereby resulting in $D_e/t = 10.2$ with $t = t_{steel} + t_{CRA}$ denoting the overall pipe wall thickness. The effects of through thickness heterogeneity are not addressed in this case study. Moreover, using the macro sections provided by Hippert [47], the girth weld geometry is approximated by a square groove weld with $2h \approx 10$ mm, which is slightly narrower than the square groove weld model of $2h = 15$ mm adopted in previous Section 5.1 but it is nevertheless sufficiently representative of the girth weld

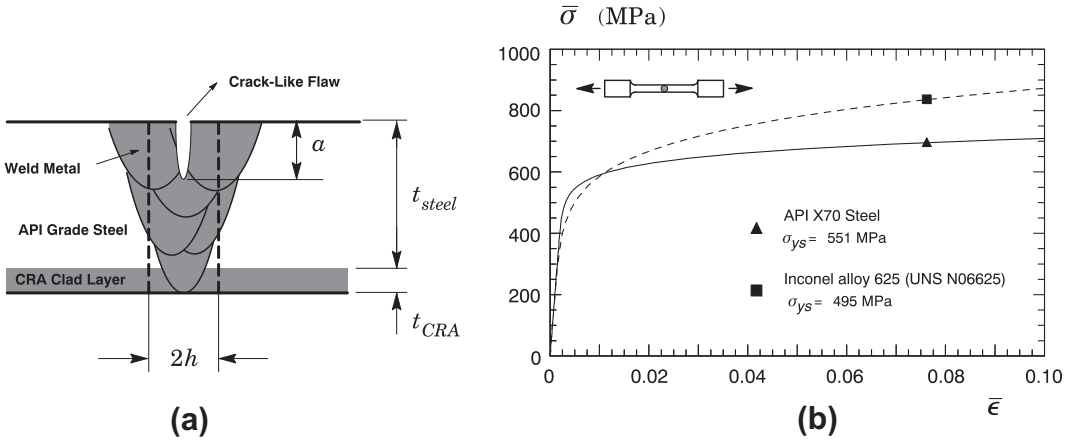

Fig. 11. (a) Representative CRA girth weld of the pipe with $D_e = 203.2$ mm (8 in), $t_{steel} = 15$ mm and clad liner thickness, $t_{CRA} = 5$ mm; (b) measured true stress vs. true strain response of the girth weld for the C–Mn pipe internally clad with UNS N06625 Alloy 625.

model from which factors h_1 are derived – recall that previous work of Paredes and Ruggieri [41] showed a relatively weak effect of the weld groove width on factor h_1 for mismatched welds. Moreover, since one of the purposes of this investigation is to study trends, the results and conclusions described next are insensitive to the exact choice of the groove width, $2h$.

The material of the external pipe is an API 5L Grade X70 pipeline steel with a higher yield stress, $\sigma_{ys} = 551$ MPa, tensile strength, $\sigma_{uts} = 660$ MPa, and relatively low hardening properties ($\sigma_{uts}/\sigma_{ys} \approx 1.20$). The inner clad layer is made of a nickel–chromium alloy 625 (UNS N06625) with the girth weld fabricated using the GTAW process with a filler metal having essentially similar metallurgical composition and mechanical properties as the clad material [47]. Tensile tests performed on the girth weld material [47] provide the yield stress, $\sigma_{ys} = 495$ MPa and tensile strength, $\sigma_{uts} = 828$ MPa, with high hardening properties ($\sigma_{uts}/\sigma_{ys} \approx 1.67$). Based on Annex F of API 579 [13], the Ramberg–Osgood strain hardening exponents describing the stress–strain response for both material is estimated as $n_{bm} = 14.2$ and $n_{wm} = 6.5$. The higher mechanical strength and superior resistance to a wide range of corrosive environments of unusual severity for this material derive from the combination of the nickel–chromium matrix with other microalloying elements such as molybdenum and niobium. Fig. 11(b) shows the measured true stress vs. true strain for both materials. It can be seen that, while the yield stress for the weld metal undermatches the yield stress for the base plate material, the higher hardening behavior of the weld metal material causes the girth weld to overmatch the base plate material after deformation levels of ~1%.

The fracture toughness value for the girth weld metal is estimated based upon DNV F108 [23] which requires fracture mechanics testing using single edge notched tensile SE(T) specimens to generate crack growth resistance data ($J - R$ curves) for ECA procedures applicable to reeling installation. Guided by preliminary fracture tests of the girth weld material [47] we take the J-value at onset of crack growth defined by $J = 400$ kJ/m^2 as the material's elastic–plastic toughness, J_{mat}. This toughness value is well in accord with previous reported crack growth resistance data for Alloy 625 materials, including weld metal and heat affected zone region.

7.2. Prediction of critical flaw sizes

Prediction of critical flaw sizes for the CRA girth weld follows from constructing the loading path (which derives from the procedure outlined previously) for each crack configuration on the K_r vs. L_r plot. Within the present context, the intersection of the loading path with the FAD assessment line (refer to Fig. 2) defines the predicted failure condition for the analyzed CRA clad pipe with undermatch girth weld. Moreover, to provide a consistent basis of comparison for the integrity assessments, the safety factors which would be applied to flaw dimensions, acting stresses and fracture toughness are set to unity.

The structural integrity analysis described here focus on critical flaw size estimates derived from four related FAD procedures and already outlined previously: (1) standard FAD assessment based on API 579 Level 2 [13] using linear elastic fracture mechanics to define the crack driving force in terms of K_I as described by Eq. (18); (2) material specific FAD curve expressed in terms of the reference stress approach outlined in Section 4.2 and described by Eq. (23) using the stress–strain response for the weld metal; (3) material specific FAD curve expressed in terms of the reference stress approach, Eq. (23), incorporating an equivalent stress–strain relationship described in Section 3.2 and (4) advanced FAD formulation incorporating the GE-EPRI evaluation methodology for J described by Eq. (24). Within the present context, the integrity assessment based on API 579 Level 2 [13] is interpreted as a baseline estimate against which other critical flaw size estimates can be compared.

The following key procedures describe the FAD assessment to determine critical flaw sizes for the CRA girth weld.

7.2.1. Standard FAD assessment based on API 579 Level 2

1. Convert J_{mat} to K_{mat} using $K_{mat} = \sqrt{J_{mat}E'}$.
2. Determine the applied bending moment, M_b, corresponding to an imposed longitudinal strain of 2% on the pipe configuration. This is the deformation level typically attained during reeling installation [3].
3. Using Annex D of API 579 [13], determine the reference stress, σ_{ref}, for the pipe configuration given by

$$\sigma_{ref} = \frac{M_b}{2R_m^2 t[2\sin\beta - (a/t)\sin\theta]}$$

where β and θ were already previously defined, and $R_m = (R_e + R_i)/2$, with R_e and R_i denoting the external and internal pipe radius.

4. Determine the applied load ratio, $\widehat{L}_r = \sigma_{ref}/\sigma_{ys}^{wm}$.
5. For a fixed crack length, $2c$, compute the applied toughness ratio, $\widehat{K}_r = K_I/K_{mat}$, for increased values of crack depth, a, until the assessment point, $(\widehat{L}_r, \widehat{K}_r)$ satisfies Eq. (18) with L_r^{max} defined by Eq. (20) thereby yielding the critical crack size, a_{cr}.

7.2.2. Material specific FAD assessment based on BS7910 Level 2B

1. Convert J_{mat} to K_{mat} using $K_{mat} = \sqrt{J_{mat}E'}$.
2. Determine the primary membrane and bending stresses, P_m and P_b, corresponding to an imposed longitudinal strain of 2% on the pipe configuration.
3. Using Annex P of BS7910 [11], determine the reference stress, σ_{ref}, based on the limit load solution of Kastner et al. [48].
4. Determine the applied load ratio, $\widehat{L}_r = \sigma_{ref}/\sigma_{ys}^{wm}$ using the stress–strain response for the weld metal.
5. For a fixed crack length, $2c$, compute the applied toughness ratio, $\widehat{K}_r = K_I/K_{mat}$, for increased values of crack depth, a, until the assessment point, $(\widehat{L}_r, \widehat{K}_r)$ satisfies Eq. (23) with L_r^{max} defined by Eq. (20) thereby yielding the critical crack size, a_{cr}.

7.2.3. Material specific FAD assessment based on BS7910 Level 2B and the ESSR procedure

1. Convert J_{mat} to K_{mat} using $K_{mat} = \sqrt{J_{mat}E'}$.
2. Determine the primary membrane and bending stresses, P_m and P_b, corresponding to an imposed longitudinal strain of 2% on the pipe configuration.
3. Determine the equivalent stress–strain relationship using Eq. (17) and the mismatch limit load solution of a plate containing a weld centerline, surface crack given by Song et al. [36].
4. Using Annex P of BS7910 [11], determine the reference stress, σ_{ref}, based on the limit load solution of Kastner et al. [48].
5. Determine the applied load ratio, $\widehat{L}_r = \sigma_{ref}/\sigma_{ys}^{wm}$ using the *equivalent* stress–strain response for the weld metal.
6. For a fixed crack length, $2c$, compute the applied toughness ratio, $\widehat{K}_r = K_I/K_{mat}$, for increased values of crack depth, a, until the assessment point, $(\widehat{L}_r, \widehat{K}_r)$ satisfies Eq. (23) with L_r^{max} defined by Eq. (20) thereby yielding the critical crack size, a_{cr}.

7.2.4. Advanced FAD assessment based on GE-EPRI

1. Use J_{mat} as the material fracture toughness.
2. Determine the applied bending moment, M_b, corresponding to an imposed longitudinal strain of 2% on the pipe configuration.
3. Determine the reference stress, σ_{ref}, using Annex D of API 579 [13], for the pipe configuration as previously defined.
4. Determine the applied load ratio, $\widehat{L}_r = \sigma_{ref}/\sigma_{ys}^{wm}$.
5. For a fixed crack length, $2c$, compute the applied toughness ratio, $\widehat{K}_r = \sqrt{J_e/J_{mat}}$, for increased values of crack depth, a, until the assessment point, $(\widehat{L}_r, \widehat{K}_r)$ satisfies Eq. (26) with L_r^{max} defined by Eq. (20) thereby yielding the critical crack size, a_{cr}.

In the above, evaluation of the applied bending moment follows from using a moment-strain relationship determined for the uncracked pipe configuration. As already described, the longitudinal bending strain, ϵ_z^b, for a pipe with outside diameter, D_e, under pure bending is given by

$$\epsilon_z^b = \frac{D_e/2}{R_b + D_e/2} \tag{34}$$

where R_b is the bending radius representing the reel drum radius in the context of ECA procedures applicable to reeling installation. As noted before, the moment-strain trajectories for cracked pipes are essentially similar to the corresponding trajectory for an uncracked pipe [31,25]. Further, within the present methodology, the longitudinal bending strain, ϵ_z^b, is effectively interpreted as a *global* measure of the applied loading that would be conventionally utilized in routine ECA applications thereby neglecting any potential effects of the mismatched girth weld on the moment-longitudinal strain response for the analyzed pipe configuration. While the merits of this approach are somewhat debatable, this considerably simplifies evaluation of the applied bending moment by performing a simpler finite element analysis for an uncracked pipe having the mechanical properties of the C–Mn steel pipeline.

Using now the ECA procedures just outlined, our exploratory analyses generate predictions of critical flaw sizes in terms of flaw depth, a_{cr}, for the CRA clad pipe with undermatch girth weld with varying crack length, $2c = 50$, 100, 150 and 200 mm, based on different assessment methodologies. Here, we note that the crack length of $2c = 200$ mm corresponds to $\theta/\pi = 0.25$ which is slightly outside the validity range of the polynomial fitting describing the variation of factor h_1 with crack geometry specified in Tables 2–4. However, as will be discussed next, the crack length, $2c$, has a relatively weak effect on the predicted critical crack size, a_{cr}, for longer flaw sizes. This behavior can be easily understood by examining the plots of h_1 with increased a/t-values showed in Figs. 7–9 in which factor h_1 displays a relatively weak sensitivity on θ/π for $\theta/\pi \geqslant 0.12$, particularly for $a/t \leq 0.3$. Essentially similar results were also obtained by Chiodo and Ruggieri [25] thereby providing support to proceed with the analysis for the case $2c = 200$ mm.

Predictions of the critical crack depth with varying crack length follow from constructing the loading path corresponding to increased crack depth (which derives from the procedure outlined in the previous sections) for each crack configuration on the K_r vs. L_r plot. Within the present context, the intersection of the loading path with the failure line described by each integrity assessment methodology defines the predicted value of a_{cr} for the analyzed cracked pipes. To illustrate the procedure, Fig. 12 displays the FAD curves and the loading paths (increasing crack depth) corresponding to a crack length of $2c = 100$ mm – the procedure to determine the a_{cr}-values for other crack lengths are similar. Here, we note that the loading path for each integrity assessment methodology follows a different pattern than the one that would otherwise be obtained from a more conventional integrity analysis in which the crack size, $2c \times a$, is fixed and the applied loading varies with the critical load (which corresponds to a critical bending moment in the present context) remaining to be determined. Because

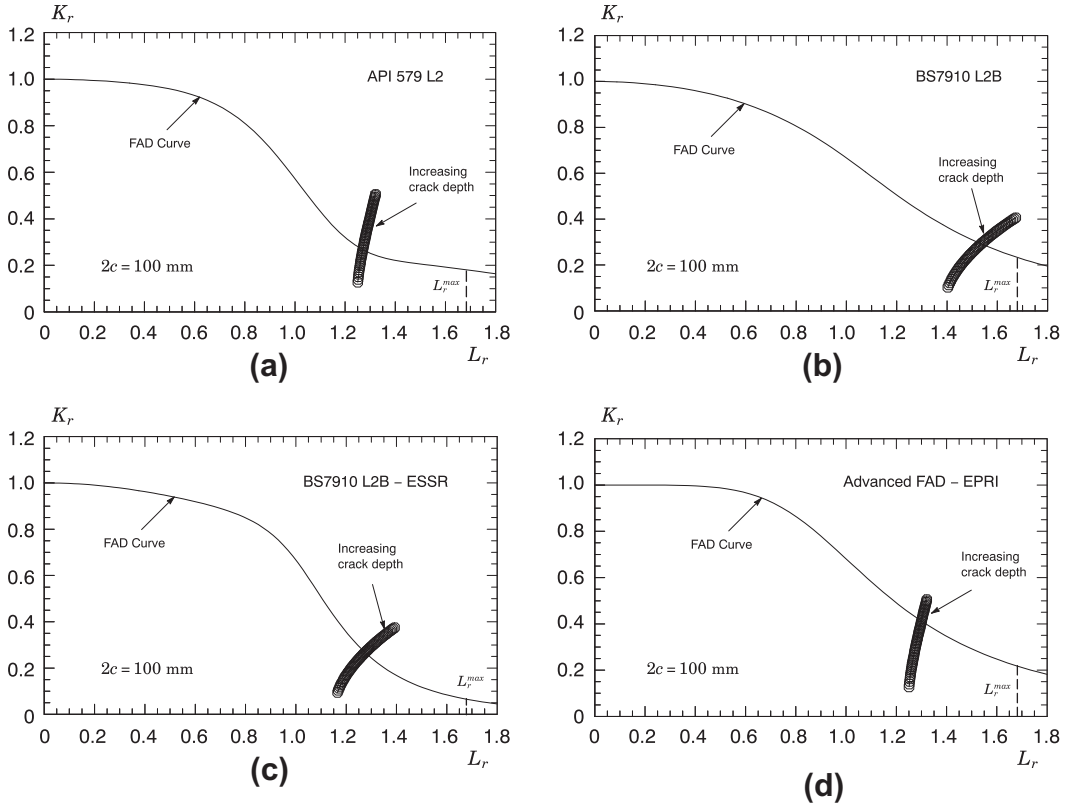

Fig. 12. FAD curves and the loading paths corresponding to a crack length of $2c = 100$ mm for each integrity assessment procedure: (a) standard FAD assessment based on API 579 Level 2; (b) material specific FAD assessment based on BS7910 Level 2B; (c) material specific FAD assessment based on BS7910 Level 2B and the ESSR procedure and (d) advanced FAD assessment based on GE-EPRI.

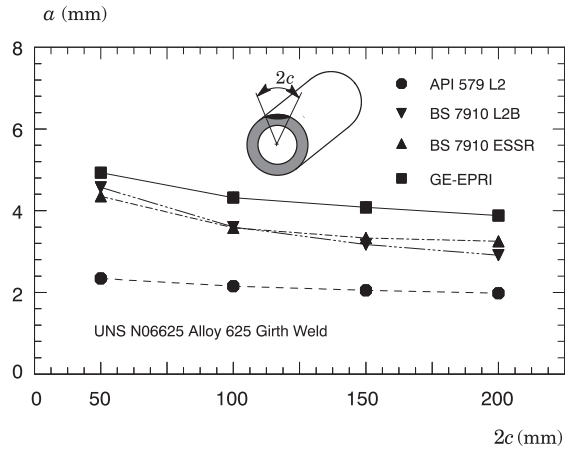

Fig. 13. Predicted critical flaw sizes for the analyzed CRA clad pipe with undermatch girth weld.

Table 5
Predicted critical flaw sizes for the analyzed CRA clad pipe with undermatch girth weld.

$2c$ (mm)	Critical crack size, a_{cr} (mm)			
	API 579 L2	BS 7910 L2B	BS 7910 ESSR	EPRI
50	2.34	4.57	4.35	4.93
100	2.15	3.60	3.58	4.32
150	2.05	3.17	3.33	4.08
200	1.98	2.91	3.25	3.88

the crack length, $2c$, and the applied (remote) bending moment, M_b, are fixed at the outset, any small increment of the crack depth, a, already shifts the corresponding point $(\widehat{K}_r, \widehat{L}_r)$ far from the axis origin of the K_r vs. L_r plot – this is precisely the result found in Fig. 12 and Fig. 13.

Table 5 compare the critical flaw sizes, a_{cr}, for the undermatch girth weld made of UNS N06625 Alloy 625. The trends are unmistakable. Integrity assessments based on more refined and accurate FAD procedures yield much larger tolerable crack size estimates. Consider for example, predictions of critical crack size for $2c = 100$ mm. The standard FAD assessment based on API 579 Level 2 [13] provides $a_{cr} = 2.15$ mm whereas the advanced FAD formulation incorporating the GE-EPRI evaluation methodology for J gives $a_{cr} = 4.32$ mm which is twice the former crack depth size.

Additional features related to these results include: (1) the crack length, $2c$, has a relatively weak effect on the predicted critical crack size (depth), a_{cr}; for example, doubling $2c$ causes a relatively small decrease in a_{cr}; (2) the material specific FAD curve expressed by Eq. (23) yields tolerable crack size estimates which are comparable, albeit slightly more conservative, to the corresponding critical crack size predictions derived from the advanced FAD procedure based on the GE-EPRI approach and (3) differences between tolerable crack size estimates derived from Eq. (23) using the stress–strain response for the weld metal and Eq. (23) incorporating an equivalent stress–strain response of the bimaterial system (base plate and weld metal) are relatively small, particularly for longer crack lengths.

8. Concluding remarks

This work describes an evaluation procedure based upon the GE-EPRI methodology and the reference stress approach to determine elastic–plastic crack driving forces (as characterized by the J-integral) in pipeline girth welds with circumferential weld centerline cracks subjected to bending load for a wide range of crack geometries and weld strength mismatch levels. The extensive 3-D finite element analyses of circumferentially surface cracked pipes performed in this study provide a new set of h_1-factors to determine J-values which enter directly into fitness-for-service (FFS) and defect assessment procedures applicable to reeling installation and other similar loading conditions. The functional dependence of factor h_1 on crack geometry and mismatch level, including the strain hardening exponent for the weld metal, is expressed in a polynomial form for simpler manipulation.

Verification studies of typical clad pipe employed in subsea flowlines having an undermatch girth weld made of a UNS N06625 Alloy 625 [1,2] compare estimates of tolerable crack sizes based upon an ECA procedure incorporating the methodologies developed here with crack size estimates obtained directly from conventional FAD methodologies. These exploratory analyses demonstrate that an advanced FAD formulation incorporating the GE-EPRI evaluation methodology reduces

significantly the conservatism that would arise from critical crack size estimates derived from a standard FAD formulation. Moreover, the present work shows that a material specific FAD curve yields tolerable crack size estimates which are comparable, albeit slightly more conservative, to the corresponding critical crack size predictions derived from the advanced FAD procedure based on the GE-EPRI approach. Here, it is of interest to note that, while a material specific FAD procedure provides conservative assessments in the case of undermatched welds, it may potentially lead to non-conservative assessment results for overmatched welds for which $M_y > 1$, so that use of the yield stress of the base metal or base plate material, σ_{ys}^{bm}, may be strongly advisable for practical assessments of overmatched welded components.

Overall, our investigation demonstrates the effectiveness of the proposed advanced FAD approach in defect assessment procedures while, at the same time, enabling additional understanding of the potential applicability of fully plastic solutions in cracked structural components. Additional studies are in progress to further validate the proposed methodology as a predictive tool for ECA procedures, including development of plastic collapse solutions for pipeline girth welds with circumferential surface cracks.

Acknowledgments

This investigation is supported by the Brazilian Council for Scientific and Technological Development (CNPq) through Grants 473975/2012-2 and 306193/2013-2 and through a Ph.D. scholarship to the first author (RFS). The authors acknowledge Petrobras for providing additional support for the work described here and for making available the experimental data. The authors are also indebted to Dr. Eduardo Hippert Jr. (Petrobras) for providing the motivation to this work and for the many helpful and insightful discussions on ECA procedures for pipelines and submarine risers.

References

[1] American Society for Testing and Materials. Standard specification for Nickel–Chromium–Molybdenum–Columbium alloy (UNS N06625) and Nickel–Chromium–Molybdenum–Silicon alloy (UNS N06219) plate, sheet, and strip, ASTM B443-00; 2009.
[2] American Society for Testing and Materials. Standard specification for Nickel–Chromium–Molybdenum–Columbium alloys (UNS N06625 and UNS N06852) and Nickel–Chromium–Molybdenum–Silicon Alloy (UNS N06219) pipe and tube, ASTM B444-06; 2011.
[3] Wästberg S, Pisarski H, Nyhus B. Guidelines for engineering critical assessments for pipeline installation methods introducing cyclic plastic strain. In: 23rd international conference on offshore mechanics and arctic engineering (OMAE). Canada: Vancouver; 2004.
[4] Chis T. The mechanics of pipeline reeling. In: Fascicle of management and technological engineering, vol. VI (XVI). Oradea University; 2007. p. 617–25.
[5] Manouchehri S, Howard B, Denniel S. A discussion of the effect of the reeled installation process on pipeline limit states. In: 18th international offshore and polar engineering conference (ISOPE). Canada: Vancouver; 2008.
[6] Manouchehri S. A discussion of practical aspects of reeled flowline installation. In: 31st international conference on ocean, offshore and arctic engineering (OMAE 2012). Rio de Janeiro (Brazil): American Society of Mechanical Engineers; 2012.
[7] Cosham A, Macdonald KA. Fracture control in pipelines under high plastic strain – a critique of DNV-RP-F108. In: 7th international pipeline conference (IPC 2008). Calgary (Canada); 2008.
[8] Hutchinson JW. Fundamentals of the phenomenological theory of nonlinear fracture mechanics. J Appl Mech 1983;50:1042–51.
[9] Anderson TL. Fracture mechanics: fundamentals and applications. 3rd ed. Boca Raton (FL): CRC Press; 2005.
[10] EDF Energy Nuclear Generation Limited. Assessment of the integrity of structures containing defects. R6 Procedure Revision 4 Including Amendment 10; 2013.
[11] British Institution. Guide to methods for assessing the acceptability of flaws in metallic structures. BS 7910; 2013.
[12] Programme EUB-E. Structural integrity assessment procedure. SINTAP; 1999.
[13] American Petroleum Institute. Fitness-for-service. API RP-579-1/ASME FFS-1; 2007.
[14] Zerbst U, Ainsworth RA, Schwalbe K-H. Basic principles of analytical flaw assessment methods. Int J Press Ves Pip 2000;77:855–67.
[15] American Petroleum Institute. Welding of pipelines and related facilities. API 1104; 2005.
[16] Canadian Standard Association. Oil & gas pipeline systems. CSA Z662; 2007.
[17] Wang Y-Y, Rudland D, Denys R, Horsley DJ. A preliminary strain-based design criterion for pipeline girth welds. In: 4th international pipeline conference (IPC 2002). Calgary (Canada); 2002.
[18] Wang Y-Y, Cheng W, McLamb M, Horsley D, Zhou J, Glover AG. Tensile strain limits of girth welds with suface-breaking defects – Part I: An analytical framework. In: Denys R, editor. 4th international conference on pipeline technology. Ostend (Belgium); 2004.
[19] Wang Y-Y, Horsley D, Cheng W, Glover AG, McLamb M, Zhou J. Tensile strain limits of girth welds with suface-breaking defects – Part II: Experimental correlation and validation. In: Denys R, editor. 4th international conference on pipeline technology. Ostend (Belgium); 2004.
[20] Wang Y-Y, Cheng W, Horsley D. Tensile strain limits of buried defects in pipeline girth welds. In: 5th international pipeline conference (IPC 2004). Calgary (Canada); 2004.
[21] Det Norske Veritas. Submarine pipeline systems. Offshore Standard OS-F101; 2000.
[22] Det Norske Veritas. Submarine pipeline systems. Offshore Standard OS-F101; 2013.
[23] Det Norske Veritas. Fracture control for pipeline installation methods introducing cyclic plastic strain. DNV-RP-F108; 2006.
[24] Macdonald KA, Cheaitani M. Engineering critical assessment in the complex girth welds of clad and lined linepipe materials. In: 8th international pipeline conference (IPC 2008). Calgary (Canada); 2010.
[25] Chiodo MSG, Ruggieri C. J and CTOD estimation procedure for circumferential surface cracks in pipes under bending. Engng Fract Mech 2010;77:415–36.
[26] Shih CF, Hutchinson JW. Fully plastic solutions and large scale yielding estimates for plane stress crack problems. Trans ASME J Engng Mater Technol – Series H 1976;98:289–95.
[27] Kumar V, German MD, Shih CF. An engineering approach to elastic–plastic fracture analysis. Tech rep. EPRI NP-1931. Electric Power Research Institute, Palo Alto (CA); 1981.
[28] Kanninen MF, Popelar CH. Advanced fracture mechanics. New York: Oxford University Press; 1985.
[29] Dowling NE. Mechanical behavior of materials: engineering methods for deformation, fracture and fatigue. 2nd ed. New Jersey: Prentice Hall; 1999.
[30] Zahoor A. Ductile fracture handbook. Tech rep. EPRI NP-6301-D. Electric Power Research Institute, Palo Alto (CA); 1989.
[31] Ostby E, Jayadevan KR, Thaulow C. Fracture response of pipelines subject to large plastic deformation under bending. Int J Press Ves Pip 2005;82:201–15.
[32] Ainsworth RA. The assessment of defects in structures of strain hardening materials. Engng Fract Mech 1984;19:633–42.
[33] Lei Y, Ainsworth RA. A *J* integral estimation method for cracks in welds with mismatched mechanical properties. Int J Press Ves Pip 1997;70:237–45.

[34] Lei Y, Ainsworth RA. The estimation of *J* in three-point-bend specimens with a crack in a mismatched weld. Int J Press Ves Pip 1997;70:247–57.
[35] British Energy Generation Limited. Assessment of the integrity of structures containing defects. R6 Procedure; 2009.
[36] Song T-K, Kim Y-J, Kim J-S, Jin T-E. Mismatch limit loads and approximate *J* estimates for tensile plates with constant-depth surface cracks in the center of welds. Int J Fract 2007;148:343–60.
[37] Dowling AR, Townley CHA. The effects of defects on structural failure: a two-criteria approach. Int J Press Ves Pip 1975;3:77–107.
[38] Harrison RP, Loosemore K, Milne I. Assessment of the Integrity of Structures Containing Defects, CEGB Report R/H/R6, Central Electricity Generating Board, UK; 1976.
[39] Det Norske Veritas. Submarine pipeline systems. Offshore Standard OS-F101; 2010.
[40] Milne I, Ainsworth RA, Dowling AR, Stewart AT. Background to and validation of CEGB Report R/H/R6 Revision 3. Int J Press Ves Pip 1988;32:105–96.
[41] Paredes M, Ruggieri C. Engineering approach for circumferential flaws in girth weld pipes subjected to bending load. Int J Press Ves Pip 2015;125:49–65.
[42] Healy B, Gullerud A, Koppenhoefer K, Roy A, RoyChowdhury S, Petti J, et al. WARP3D: 3-D nonlinear finite element analysis of solids for fracture and fatigue processes. Tech rep. University of Illinois at Urbana-Champaign; 2014. <http://code.google.com/p/warp3d>.
[43] Moran B, Shih CF. A general treatment of crack tip contour integrals. Int J Fract 1987;35:295–310.
[44] Silva LAL, Cravero S, Ruggieri C. Correlation of fracture behavior in high pressure pipelines with axial flaws using constraint designed test specimens – Part II: 3-D effects on constraint. Engng Fract Mech 2006;76:2123–38.
[45] Ruggieri C. FRACTUS2D: numerical computation of fracture mechanics parameters for 2-D cracked solids. Tech rep. University of Sao Paulo; 2011.
[46] Wolfran S. The mathematica book. 5th ed. Wolfran Media; 2003.
[47] Hippert E. Private communication; 2013.
[48] Kastner W, Röhrich E, Schmitt W, Steinbuch R. Critical crack sizes in ductile piping. Int J Press Ves Pip 1981;9:197–219.